ARCHIVES of FOUNDRY ENGINEERING

ISSN (1897-3310)
Volume 17
Issue 2/2017

101 – 106

19/2

Published quarterly as the organ of the Foundry Commission of the Polish Academy of Sciences

Physicochemical Properties of Silicon Cast Iron

M. Stawarz [a,] *, W. Kajzer [b], A. Kajzer [b], M. Dojka [a]
[a] Department of Foundry Silesian University of Technology,
ul. Towarowa 7, 44-100 Gliwice Poland
[b] Department of Biomaterials and Medical Devices Engineering **,** Silesian University of Technology
ul. Roosevelta 40, 41-800 Zabrze, Poland
* Corresponding author. E-mail address: marcin.stawarz@polsl.pl

Received 28.11.2016; accepted in revised form 20.12.2016

Abstract

The article presents results of pitting corrosion studies of selected silicon cast irons. The range of studies included low, medium and high silicon cast iron. The amount of alloying addition (Si) in examined cast irons was between 5 to 25 %. Experimental melts of silicon cast irons [1-3] were conducted in Department of Foundry of Silesian University of Technology in Gliwice and pitting corrosion resistance tests were performed in Faculty of Biomedical Engineering in Department of Biomaterials and Medical Devices Engineering of Silesian University of Technology in Zabrze. In tests of corrosion resistance the potentiostat VoltaLab PGP201 was used. Results obtained in those research complement the knowledge about the corrosion resistance of iron alloys with carbon containing Si alloying addition above 17 % [4-6]. Obtained results were supplemented with metallographic examinations using scanning electron microscopy. The analysis of chemical composition for cast irons using Leco spectrometer was done and the content of alloying element (silicon) was also determined using the gravimetric method in the laboratory of the Institute of Welding in Gliwice. The compounds of microstructure was identify by X-ray diffraction.

Keywords: Pitting corrosion, Alloy cast iron, SiMo, Silicon cast iron

1. Introduction

Alloying elements can play a main role in the sensitivity of cast irons to corrosion attack. The alloying elements generally used to increase the corrosion resistance of cast irons include silicon, nickel, copper, molybdenum and chromium [4]. Silicon is the most important alloying element used to improve the corrosion resistance of cast irons [4-7]. Silicon is generally not considered an alloying element in cast ions until levels exceed 3% [4-5]. Silicon levels between 3 and 14% offer some increase in corrosion resistance to the alloy, but above about 14% Si, the corrosion resistance of the cast iron increases significantly [4]. Silicon levels up to 17% have been used to enhance the corrosion resistance of the alloy further, but silicon levels over 16% make difficult to manufacture [1-7]. The main use of silicon cast iron are: anodes for corrosion protection, pump cases for transport of aggressive fabrics, inserts in valves for transport of aggressive fluids, drains in chemical companies, hospitals and laboratories, pipes, nozzles in mixers and blenders, bearings in corrosive and or higher temperature circumstances [7]. The main applications of SiMo cast iron (with 5% Si content) are: exhaust manifolds for combustion engines, gas turbine components, moulds for casting of titanium, brass and zinc alloys, holders for heat treatment (cyclic temperature changes), elements of furnaces for heat treatment [8-11].

Figures 1 and 2 show the effect of silicon content on the corrosion rate according to the corrosive environment and temperature.

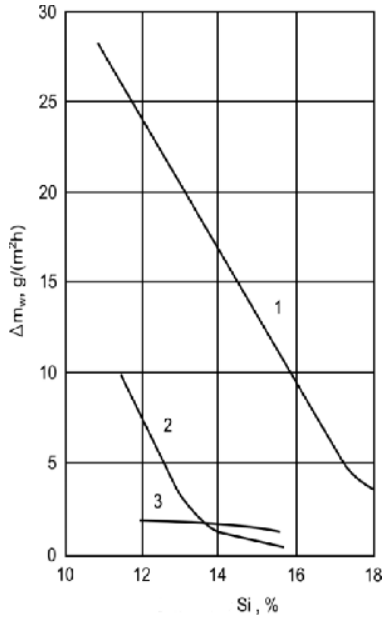

Fig. 1. Corrosion rates of high silicon cast irons as a function of silicon content and corrosive media. 1 – 35 % HCl solution, temp. 80°C, 2 – 40 % H_2SO_4 solution, temp. 60°C, 3 – 20 % HNO_3 solution, temp. 60°C [5]

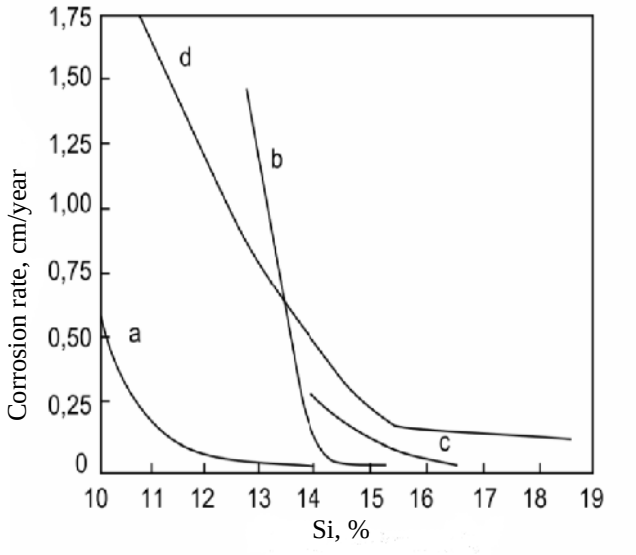

Fig. 2. Corrosion rates of high silicon cast irons as a function of silicon content and corrosive media.
a – 70% HNO_3 solution, boiling point, b – 20% H_2SO_4 solution, boiling point, c – 10% HNO_3 solution, boiling point, d – 10% HCl solution, temp. 80°C [12]

High resistance to wear, very good resistance to corrosion and the additional advantage of this material is the low production cost. Was the reason for research (alloys with containing more than 17% Si) in terms of corrosion resistance.

2. Description of the work methodology

Experimental melts were conducted in the induction furnace with medium frequency. The charge consisted of steel scrap with low sulphur content. Other ingredients added during the melting was Ranco carburizer, ferrosilicon FeSi75, and FeMo65 rich alloy (for SiMo ductile cast iron). The spheroidization process (for SiMo ductile iron) of cast iron was conducted in the bottom of the ladle, after covering the nodulizing agent by pieces of steel scrap [13]. Magnesium rich alloy used in the studies was FeSiMg5RE. The charging materials were melted down, the carburizer was introduced and then the metal bath was overheated. The next step was liquid alloy cooling (slowly, along with furnace cooling) down to 1200°C. This operation's goal was to remove all gases dissolved in molten metal [2]. Then the liquid metal bath was heated up to1350°C. Liquid alloy was poured into hot foundry ladle and then poured into shell moulds. The test set up for potentiodynamic corrosion test was presented on Fig 3:

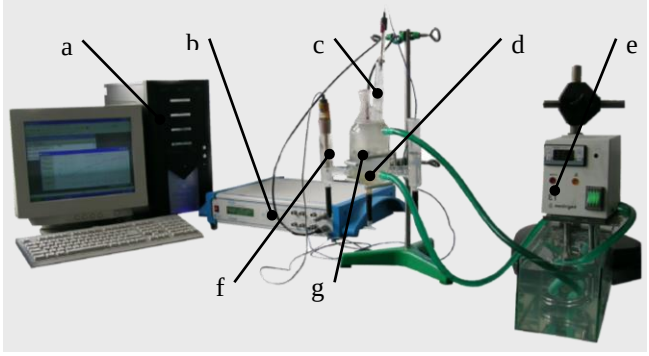

Fig. 3. The measuring set used in the study[14-16]:
a – set of recording graphs anodic polarization curves,
b – potentiostat VoltaLab® PGP201, c – reference electrode - impregnated calomel electrode (NEK) type KP-113,
d – electrochemical cell test, e – thermostat Medlingen,
f – secondary electrode – platinum electrode type PtP – 201,
g – anode - test sample

As a corossive environment for studies the aqueous solution of 3% NaCl was used.

The corrosion tests started with establishing the open circuit potential E_{OCP} at currentless conditions during the time T = 120 min. The polarization curves were recorded starting with the initial potential value, $E_{init} = E_{OCP} - 100$ mV. The potential changed along the anode direction at the rate of 3 mV/s.Once the anodic current density reached the value of 1 mA/cm^2, the polarization direction was changed. On the basis of the obtained curves the corrosion potential E_{corr} was determined, and the value of the polarization resistance R_p and corrosion current i_{corr} were calculated with the use of the Stern and Tafel methods [14-16].

3. Research results

Table 1 presents the results of chemical analysis of tested experimental alloys. Presented chemical composition is the result from the analysis on Leco spectrometer, while the carbon and sulphur content was obtained using Leco analyser of carbon and sulphur. The data in Table 1 for C and S was corrected. Si content in the tested alloys was examined by gravimetric method in the Welding Institute in Gliwice.

Table 1.
Chemical composition of silicon cast iron

Alloy	Element content, % wt.						
No.	C	Si	Mo	P	Mn	S	Mg
1	3.04	4.94	1.09	0.022	0.421	0.005	0.031
2	1.39	10.27	0.01	0.023	0.304	0.013	0.00
3	0.42	16.13	0.02	0.019	0.339	0.001	0.00
4	0.52	17.92	0.02	0.018	0.341	0.003	0.00
5	0.12	26.23	0.01	0.021	0.329	0.001	0.00

Figures 4-8 shows a comparison of microstructure of examined alloys. On Figure 4 can be noticed precipitation of nodular graphite in ferritic matrix. X-ray diffraction shown the present of molybdenum on the grain boundaries (not visible in the photograph).

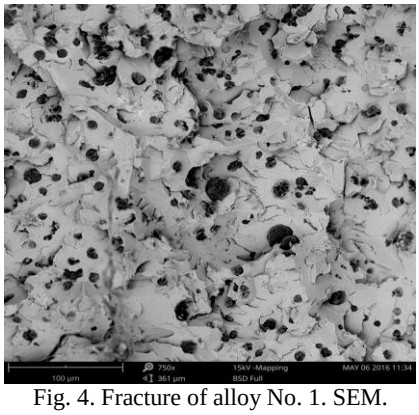

Fig. 4. Fracture of alloy No. 1. SEM.

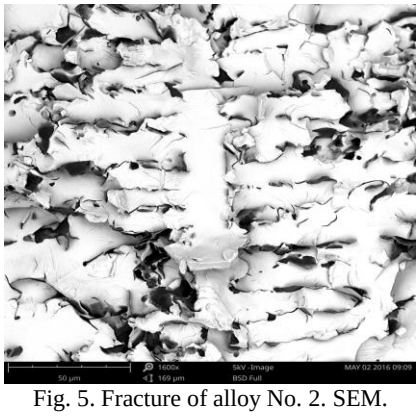

Fig. 5. Fracture of alloy No. 2. SEM.

Figure 5 presents microstructure of cast iron with 10.27% Si content. Flake interdendritic graphite in ferritic matrix is clearly visible in this photograph.

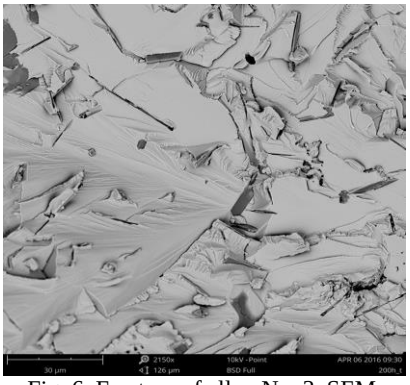

Fig. 6. Fracture of alloy No. 3. SEM.

Figure 6 presents microstructure of cast iron with 16.13% Si content. The compounds present in microstructure were classified using X-ray diffraction as silicon ferrite and intermetallic phases Fe_3Si, Fe_5Si_3.

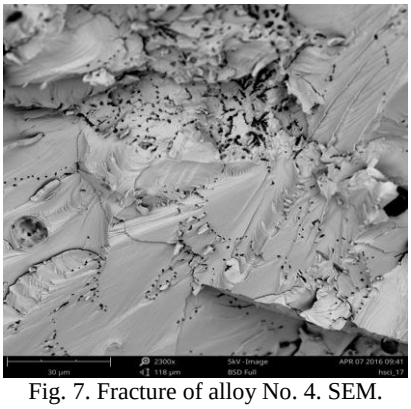

Fig. 7. Fracture of alloy No. 4. SEM.

Figure 7 presents microstructure of cast iron with 17.92% Si content. The components present in microstructure were classified using X-ray diffraction as silicon ferrite, graphite and intermetallic phases Fe_3Si, Fe_5Si_3 and SiC.

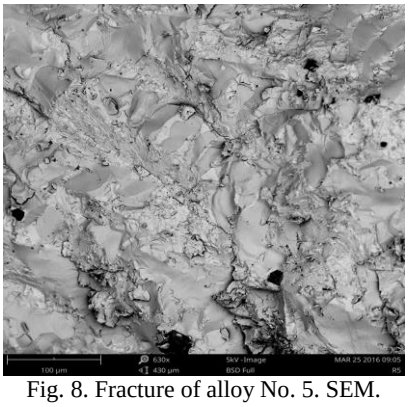

Fig. 8. Fracture of alloy No. 5. SEM.

Figure 8 present microstructure of cast iron with 26.23% Si content. The compounds present in microstructure were classified using X-ray diffraction as silicon ferrite and intermetallic phases FeSi, Fe_3Si, Fe_5Si_3 and SiC.

Results of potentiodynamic tests of pitting corrosion resistance were shown in Table 2 and Figure 9.

Table 2.
Results of potentiodynamic tests – mean values

Alloy No.	Si, % wt	*E_{corr}, mV	*STD	*E_b, mV	STD	*E_{cp}, mV	STD	*E_{tr}, mV	STD	*R_p, kΩ·cm^2	STD	*I_{corr}, μA/cm^2	STD
1	4.94	-705	±2.5	-584	±9.6	-643	±2.0	-	-	1.28	±0.09	11.0	±1.1
2	10.27	-688	±3.0	-497	±1.2	-653	±14.4	-	-	1.82	±0.90	13.8	±6.3
3	16.13	-90	±8.7	-	-	-	-	1490	±13.5	41.6	±8.03	1.6	±0.6
4	17.92	-262	±1.0	-	-	-	-	1488	±16.2	30.0	±29.9	4.3	±4.3
5	26.23	-167	±9.6	-	-	-	-	1472	±17.0	102.8	±22.2	0.2	±0.1

* Description of symbols used in the table: E_{corr} – corrosion potential, E_b – breakdown potential, E_{cp} – repassivation potential, E_{tr} – transpassivation potential, R_p – polarization resistance, I_{corr} – corrosion current, STD – standard deviation.

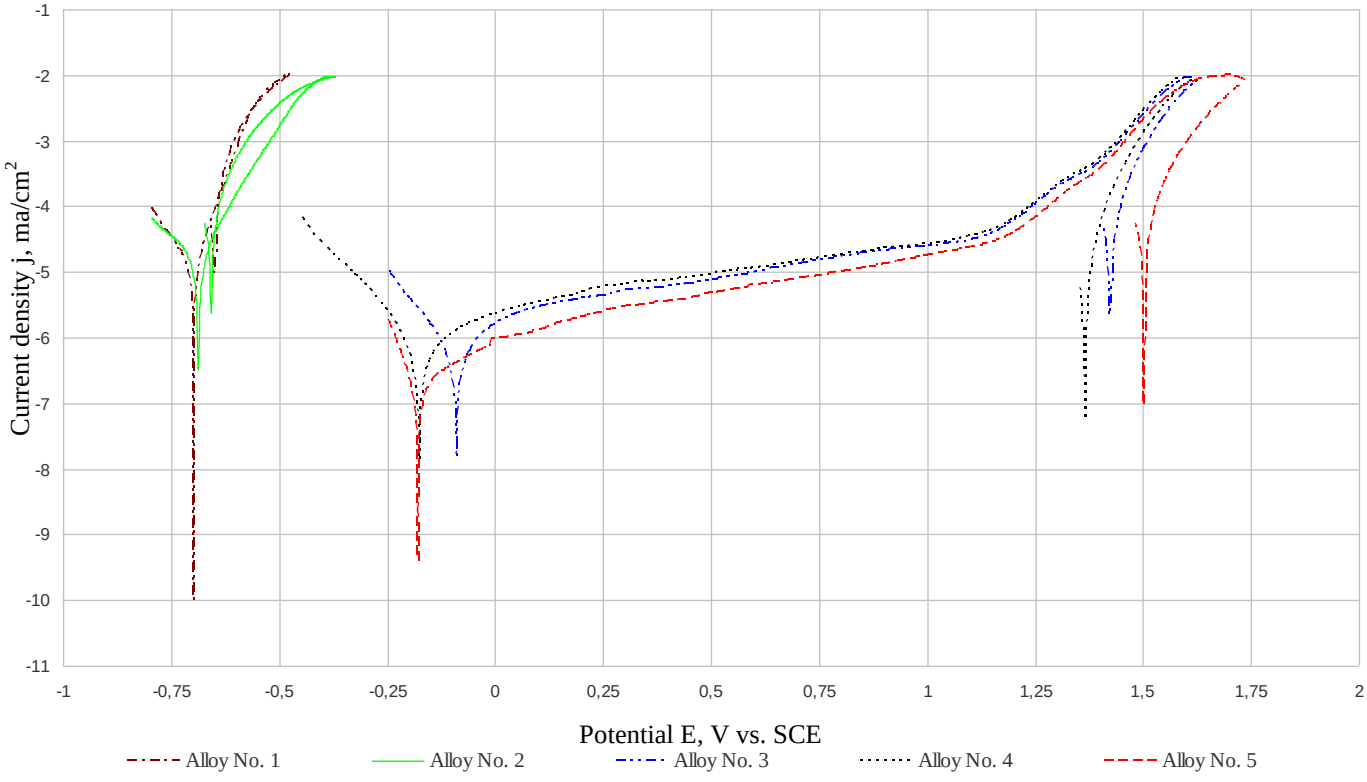

Fig. 9. Polarization curves for the tested alloys

Figures 10-12 present the surfaces of the samples after pitting corrosion resistance testings. Photos were taken with the use of Phenom ProX scanning electron microscope. It was decided to present surfaces of samples for Alloy No. 1 and Alloy No. 2 and for the sample Alloy No. 5. On the surfaces of the samples Alloy No. 1 and Alloy No. 2 (Fig. 10-11) clear defects of pitting type were observed with high amount of corrosion products on the verges of this defects.

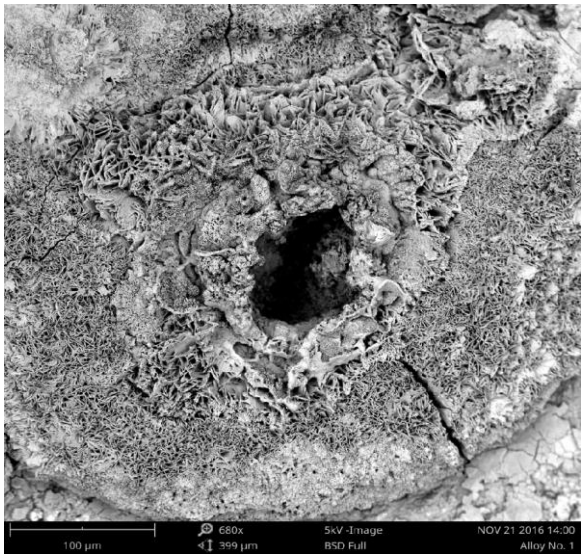

Fig. 10. Pitting defect on the surface of the sample after corrosion resistance testing performer using potentiostat. Alloy No. 1. SEM

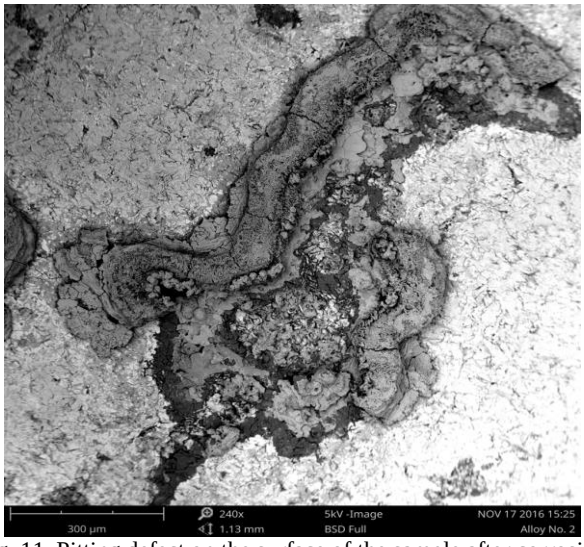

Fig. 11. Pitting defect on the surface of the sample after corrosion resistance testing performer using potentiostat. Alloy No. 2. SEM

Figure 12 presents the surface of sample Alloy No. 5. No signs of pitting corrosion were observed on this sample, the whole surface of the sample is covered with passive layer.

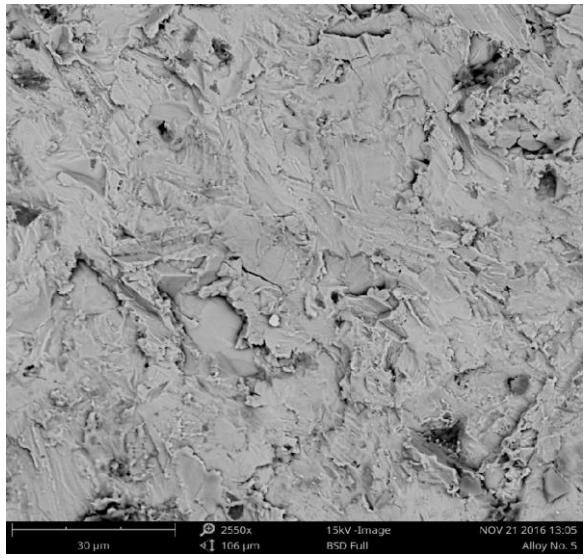

Fig. 12. Pitting defect on the surface of the sample after corrosion resistance testing performer using potentiostat. Alloy No. 5. SEM

4. Conclusions

Basing on the results of studies concluded that the corrosion potentials E_{corr} for samples of alloy 1 and 2 are between -705 mV to -688 mV while the corrosion potentials for samples of alloy 3-5 are between -268 mV do -90 mV. For samples 1 and 2 concluded the low value of breakdown potential E_b and repassivation E_{cp} (table 2) which says about the absence of pitting corrosion resistance in those cases. However, for other tested alloys the transpassivation potential E_{tr} has got a preferred value, which is about 1490 mV for alloys with 16.13, 17.92 and 26.23 % Si content (table 2). Besides, the addition of silicon added into analysed melts contributed to the increase of polarization resistance value (Fig. 11) and the decrease of corrosion current value in comparison to samples from alloys 1 and 2. The long plato section on polarization graph (Fig. 10) indicates the presence of passive layer on the surface of examined alloys (3-5) which significantly improves the corrosion resistance of high silicon cast iron in comparison to low and medium silicon cast irons. Taking into account obtained parameters the best pitting corrosion resistance is characterised by alloy 5 with 26,23 % of Si. Studies [5, 12] state about positive influence of Si on the decrease of the corrosion speed. This is confirmed by the results of potentiodynamic, for witch it was stated that for alloys with Si content between 16 and 26% transpassivation potential occurs alongside with higher values of polarizing in comparison to the alloys with Si content at levels of 4.94 and 10.27% (Alloy No. 1., and Alloy No. 2).

The confirmation of obtained results (Fig. 9) of potentiodynamic testings are the photos of pitting type defects (Fig. 10, Fig. 11) on the surface of samples Alloy No. 1 and Alloy No. 2, while for the melts with the content of Si above 16% compact passive layer and no pitting type defects were noticed (Fig. 12).

References

[1] Nuckowski, P.M., Kwaśny, W., Rdzawski, Z., Głuchowski, W.& Pawlyta, M. (2016). Influence of the Repetitive Corrugation on the Mechanism Occurring During Plastic Deformation of CuSn6 Alloy. *Archives of Metallurgy and Materials.* 61(3), 1261-1264.

[2] Stawarz, M., Janerka, K., Jezierski, J., Szajnar, J. (2014). Thermal effect of phase transformations in high silicon cast iron. In Metal 2014: 23rd International Conference on Metallurgy and Materials. Ostrava: TANGER 2014 (pp. 123-128).

[3] Stawarz, M., Gromczyk, M., Jezierski, J., Janerka, K. (2015). Analysis of the high silicon cast iron crystallization process with TDA method. In Metal 2015: 24th International Conference on Metallurgy and Materials. Ostrava: TANGER 2015, (pp. 42-47).

[4] Korb, L.J. & Olson, D.L. (1992*). Corrosion.* Volume 13 (9th ed.). International ASM Handbook., 1384 p.

[5] Podrzucki, C. (1991). *Cast Iron*. Volume 2. Kraków: ZG Stop. 298 p. (*in Polish*)

[6] Stefanescu, D.M. (1998). *Casting*. Volume 15. (4th ed.). International ASM Handbook.

[7] Henderieckx, G.D. (2009). *Silicon Cast Iron*. Gietech BV.

[8] Delprete, C., Sesana, R. & Vercelli, A. (2010). Multiaxial damage assessment and life estimation: application to an automotive exhaust manifold. *Procedia Engineering.* 2, 725-734. DOI:10.1016/j.proeng.2010.03.078

[9] Matteis, P., Scavino, G., Castello, A. & Firrao, D. (2014). High temperature fatigue properties of a Si-Mo ductile cast iron. *Procedia Materials Science.* 3, 2154-2159. DOI: 10.1016/j.mspro.2014.06.349.

[10] Guzik, E. & Wierzchowski, D. (2012) Using cored wires injection 2PE-9 method in the production of ferritic Si-Mo ductile iron castings. *Archives of Foundry Engineering.* 12(4), 53-56.

[11] Magnusson Åberg, L. & Hartung, C. (2012). Solidification of SiMo nodular cast iron for high temperature applications. *Trans Indian Inst Met.* 65(6), 633-636. DOI:10.1007/s12666-012-0216-8.

[12] Shreira L.L. (1966). *Corrosion*. Volume 1. Warszawa: Scientific and Technical Publishing. (*in Polish*).

[13] Stawarz, M. (2017). SiMo Ductile Iron Crystallization Process. *Archives of Foundry Engineering.* 17(1), 147-152. DOI: 10.1515/afe-2017-0027.

[14] Kajzer, A., Kajzer, W., Gołombek, K., Knol, M., Dzielicki, J. & Walke, W. (2016). Corrosion resistance, eis and wettability of the implants made of 316 LVM steel used in chest deformation treatment. *Archives of Metallurgy and Materials*. 61(2a), 767-770. DOI:10.1515/amm-2016-0130.

[15] Szewczenko, J., Marciniak, J., Kajzer, W. & Kajzer, A. (2016). Evaluation of corrosive resistance of titanium alloys used for medical implants. *Arch. Metall. Mater*. 61(2a), 695-700. DOI:10.1515/amm-2016-0118.

[16] Basiaga, M., Kajzer, W., Walke, W., Kajzer, A. & Kaczmarek, M. (2016). Evaluation of physicochemical properties of surface modified Ti6Al4V and Ti6Al7Nb alloys used for orthopedic implants *Materials Science and Engineering.* C(68), 851-860. DOI:10.1016/j.msec. 2016.07.042.